Tracer Monitored Titrations: Measurement of Total Alkalinity

ARTICLE *in* ANALYTICAL CHEMISTRY · APRIL 2006

Impact Factor: 5.64 · DOI: 10.1021/ac0516133 · Source: PubMed

3 AUTHORS, INCLUDING:

Andrew Dickson
University of California, San Diego
99 PUBLICATIONS **6,517** CITATIONS
SEE PROFILE

Mike DeGrandpre
University of Montana
84 PUBLICATIONS **1,949** CITATIONS
SEE PROFILE

Anal. Chem. **2006,** *78,* 1817−1826

Tracer Monitored Titrations: Measurement of Total Alkalinity

Todd R. Martz,[†] Andrew G. Dickson,[‡] and Michael D. DeGrandpre*,[†]

Department of Chemistry, The University of Montana, 32 Campus Drive, Missoula, Montana 59812, and Marine Physical Laboratory, Scripps Institution of Oceanography, University of California, San Diego, 9500 Gilman Drive, La Jolla, California 92093-0244

We introduce a new titration methodology, tracer monitored titration (TMT), in which analyses are free of volumetric and gravimetric measurements and insensitive to pump precision and reproducibility. Spectrophotometric monitoring of titrant dilution, rather than volume increment, lays the burden of analytical performance solely on the spectrophotometer. In the method described here, the titrant is a standardized mixture of acid−base indicator and strong acid. Dilution of a pulse of titrant in a titration vessel is tracked using the total indicator concentration measured spectrophotometrically. The concentrations of reacted and unreacted indicator species, derived from Beer's law, are used to calculate the relative proportions of titrant and sample in addition to the equilibrium position (pH) of the titration mixture. Because the method does not require volumetric or gravimetric additions of titrant, simple low-precision pumps can be used. Here, we demonstrate application of TMT for analysis of total alkalinity (A_T). High-precision, high-accuracy seawater A_T measurements are crucial for understanding, for example, the marine $CaCO_3$ budget and saturation state, anthropogenic CO_2 penetration into the oceans, calcareous phytoplankton blooms, and coral reef dynamics. We present data from 286 titrations on three types of total alkalinity standards: Na_2CO_3 in 0.7 mol kg·soln^{-1} NaCl, NaOH in 0.7 mol kg·soln^{-1} NaCl, and a seawater Certified Reference Material (CRM). Based on Na_2CO_3 standards, the accuracy and precision are ±0.2 and ±0.1% (4 and 2 μmol kg·soln^{-1} for A_T ~2100−2500 μmol kg·soln^{-1}, n = 242), using low-precision solenoid pumps to introduce sample and titrant. Similar accuracy and precision were found for analyses run 42 days after the initial experiments. Excellent performance is achieved by optimizing the spectrophotometric detection system and relying upon basic chemical thermodynamics for calculating the equivalence point. Although applied to acid−base titrations in this paper, the approach should be generally applicable to other types of titrations.

There is great demand for simplified titrations that can be automated for operator-free applications in industrial, medical and environmental monitoring, and research. Conventional titration methods use calibrated volumetric flasks and titration cells or gravimetry to quantify sample and calibrated burets or pipets to dispense titrant. Automated systems typically use volumetric analysis because gravimetric measurements of sample and titrant are very difficult to automate.[1] These volumetric techniques have been automated using in-line pipets[2] and sample loops[3] for sample quantification along with motorized burets[2] and coulometry[3] for titrant quantification. Fully automated robotic systems have also been developed.[4] These methods achieve excellent accuracy and precision but require careful empirical calibration of each vessel in addition to several sophisticated motorized components (pumps, valves, piston burets). Some automated methods, such as flow injection analysis,[5] sequential injection analysis,[6] continuous on-line end point monitoring[7,8] and a variety of unsegmented batch titrations,[9,10] do not require volumetric or gravimetric measurements. These titrations use peak width measurements with a time abscissa or directly incorporate flow rate into the end point calculation. These "volumetric−gravimetric-free" techniques are therefore very dependent upon flow rate and, to obtain the best data, require use of high-precision pumps and the repeated introduction of standards to compensate for pump fluctuations. The development of an automated method, free of volumetric and gravimetric measurements and high-precision pumps, would significantly simplify titrimetric analysis making it more amenable to unattended operation.

Here we present a new method, tracer monitored titration (TMT), which quantifies the relative proportions (based on dilution factors) of titrant and sample through a chemical tracer (colorimetric indicator) in the titrant. The dilution factors are used in the equivalence point calculation in place of physically metered volumes, masses, flow rates, or peak width (time). We developed the TMT method for analysis of seawater total alkalinity (A_T). In the application described here, the titrant is a standardized mixture of an acid−base indicator and HCl. Measurement of the individual

* To whom correspondence should be addressed. E-mail: michael.degrandpre@umontana.edu.

[†] The University of Montana.

[‡] University of California, San Diego.

(1) Yao, W.; Byrne, R. H. *Deep-Sea Res. I* **1998**, *45*, 1383−1392.
(2) Roche, M. P.; Millero, F. J. *Mar. Chem.* **1998**, *60*, 85−94.
(3) Liang, Y. Y. *Anal. Chem.* **1990**, *62*, 2504−2506.
(4) Metrohm Automated Titration Systems (MATi): www.metrohm.com.
(5) Ruzicka, J. *Flow Injection Analysis*, 2nd ed.; J. Wiley: New York, 1988.
(6) Fletcher, P. J.; van Staden, J. F. *Anal. Chim. Acta* **2003**, *485*, 187−194.
(7) Tanaka, H.; Dasgupta, P. K.; Huang, J. *Anal. Chem.* **2000**, *72*, 4713−4720.
(8) Watanabe, A.; Kayanne, H.; Nozaki, K.; Kato, K.; Negishi, A.; Kudo, S.; Kimoto, H.; Tsuda, M.; Dickson, A. G. *Mar. Chem.* **2004**, *85*, 75−87.
(9) Almeida, C. M. N. V.; Lapa, R. A. S.; Lima, J. L. F. C.; Zagatto, E. A. G.; Araujo, M. C. U. *Anal. Chim. Acta* **2000**, *407*, 213−223.
(10) Korn, M.; Gouveria, L. F. B. P.; de Oliveria, E.; Reis, B. F. *Anal. Chim. Acta* **1995**, *313*, 177−184.

10.1021/ac0516133 CCC: $33.50
Published on Web 02/14/2006

concentration of each indicator species allows approximation of titrant and sample dilution factors (from observed total indicator concentration) in addition to the pH of the titration mixture (from the ratio of indicator concentrations).

Spectrophotometry has been used as a detection method in acid−base titrations for many years. Optical absorbance measurements are potentially superior to potentiometric measurements because electrodes are prone to large systematic errors and unpredictable drift. A simple photometric titration is carried out by adding a small, nonquantitative amount of indicator to the titration solution and monitoring optical absorbance at a single wavelength.[11] The maximum slope or inflection of the absorbance versus volume of titrant curve gives the end point. More sophisticated spectrophotometric methods use quantitative addition of indicator to the titration solution, accurate absorbance measurements at two wavelengths, and subsequent calculation of solution pH with correction for pH perturbation by the acid−base indicator.[1] The equivalence point is determined from the volumes (or masses) of titrant and sample and the pH of the titration mixture, as determined by the indicator. To our knowledge, TMT is the first titration method that uses the indicator to simultaneously quantify the total titrant added and pH after each titrant addition.

Our primary interest in developing a simplified titration system is driven by our research on the marine inorganic carbon cycle. Since the Geochemical Ocean Sections Study (GEOSECS) began in the late 1960s, A_T has been one of the most commonly measured parameters in most large-scale oceanographic CO_2 system studies. Between 1991 and 1998, the Joint Global Ocean Flux Study (JGOFS), World Ocean Circulation Experiment (WOCE), and Ocean Atmosphere Carbon Exchange Study (OACES) sampled CO_2 parameters at more than 12 000 depth-resolved hydrographic stations, resulting in over 350 000 discrete measurements.[12] Total dissolved inorganic carbon (C_T) and A_T were the most commonly measured CO_2 system parameters in these studies.[12] For example, high-quality, high-coverage A_T measurements are useful for estimating anthropogenic CO_2 penetration in the ocean,[13,14] balancing the marine calcium carbonate budget,[15,16] constraining ocean−atmosphere CO_2 fluxes,[17] separating the processes of photosynthesis and calcification in phytoplankton blooms,[18] and understanding coral reef carbon budget,[19] effects of ocean acidification.[20] and bioerosion.[21]

Many of these applications require A_T precision and accuracy of at least 0.1%[22] or, more specifically, a ~2 μmol kg·soln^{-1} resolution out of 2000 μmol kg·soln^{-1} on a 0.7 mol kg·soln^{-1} salt background. In addition, titrations must be performed continuously at sea on a medium to high frequency (~15 min or less). All data collected during the GEOSECS, JGOFS, WOCE, and OACES projects were obtained from semiautomated batch titrations that require a full-time operator. A few researchers have successfully built fully automated seawater A_T systems. Roche and Millero[2] developed a spectrophotometric system that achieved accuracy and precision of ~0.1%. Most recently, Watanabe et al.[8] developed an automated potentiometric method based on daily calibrations of an electrode's response to standards. Both of these systems rely, however, on accurate and precise volumetric delivery. The oceanographic community would greatly benefit from a simpler, faster, and less expensive titration system for shipboard studies. Furthermore, a simplified system could eventually be adapted for autonomous in situ measurements. An autonomous instrument for A_T, similar to those already developed by us for pCO_2[23] and pH,[24] would allow continuous A_T monitoring from moorings or autonomous floats, in place of the current shipboard methods.

In this study, an automated TMT system used a standardized mixture of HCl, bromocresol green (BCG), and NaCl to analyze alkaline samples at concentrations and ionic strengths similar to seawater. Simple solenoid pumps (with volume reproducible to only 10%) flushed sample and made additions of titrant, while spectrophotometric measurements simultaneously estimated total indicator concentration and pH in a stirred optical cell. To test the TMT method for seawater A_T applications, we analyzed Na_2CO_3 solutions in 0.7 mol kg·soln^{-1} NaCl. In addition, we titrated solutions of NaOH in 0.7 mol kg·soln^{-1} NaCl and a seawater Certified Reference Material (CRM). In this initial proof-of-concept evaluation, we present the TMT theory, examine the sensitivity of the method to experimental parameters using a theoretical model, and present the results from analysis of 286 alkalinity measurements obtained over a 42-day period.

THEORY

Calculation of the Titrimetric Equivalence Point. Here, we derive the theory of TMT specifically for acid−base titrations. Throughout the paper, the HCl−indicator mixture is denoted with the subscript a/i and the concentration unit is mols per kilogram of solution (mol kg·soln^{-1}). As explained by Dickson,[25] A_T is a measurable aqueous parameter describing the excess of proton acceptors over proton donors where proton acceptors are bases formed from weak acids with a dissociation constant $K \leq 10^{-4.5}$ at 25 °C and ionic strength, $I = 0$ mol kg·soln^{-1}, and proton donors are acids with $K > 10^{-4.5}$, at 25 °C and $I = 0$. During any point in a titration, the excess of proton acceptors is represented by

$$\frac{C_{a/i}M_{a/i} - A_T M_s}{M_{a/i} + M_s} = \sum_{i=1}^{n}[HA_i] - \sum_{j=1}^{m}[B_j] \qquad (1)$$

where $C_{a/i}$ is the acidity of the a/i titrant due to both HCl and indicator, $M_{a/i}$ is mass of titrant added, M_s is sample mass, and

(11) Day, R. A., Jr.; Underwood, A. L. *Quantitative Analysis*, 6th ed.; Prentice Hall: Englewood Cliffs, NJ, 1991.
(12) Carbon Dioxide Information Analysis Center (CDIAC), Global Ocean Data Analysis Project (GLODAP), http://cdiac.esd.ornl.gov/oceans/glodap/Glodap_home.htm.
(13) Gruber, N.; Sarmiento, J. L.; Stocker, T. F. *Global Biogeochem. Cycles* **1996**, *10*, 809−837.
(14) Sabine, C. L.; et al. *Science* **2004**, *305*, 367−371.
(15) Milliman, J. D.; Troy, P. J.; Balch, W. M.; Adams, A. K.; Li, Y. H.; Mackenzie, F. T. *Deep-Sea Res. I* **1999**, 1653−1669.
(16) Feely, R. A.; et al. *Global Biogeochem. Cycles.* **2002**, *16*, 91-1−91-12.
(17) Gloor, M.; Gruber, N.; Sarmiento, J.; Sabine, C. L.; Feely, R. A.; Rodenbeck, C. *Geophys. Res. Lett.* **2003**, *30*, 10-1−10-4.
(18) Bates, N. R.; Michaels, A. F.; Knap, A. H. *Mar. Chem.* **1996**, *51*, 347−358.
(19) Suzuki, A.; Kawahata, H. *Tellus* **2003**, *55B*, 428−444.
(20) Langdon, C.; Takahashi, T.; Sweeney, C.; Chipman, D.; Goddard, J.; Marubini, F.; Aceves, H.; Barnett, H.; Atkinson, M. J. *Global Biogeochem. Cycles* **2000**, *14*, 639−654.
(21) Lazar, B.; Loya, Y. *Limnol. Oceanogr.* **1991**, *36*, 377−383.
(22) Dickson, A. G.; Riley, J. P. *Mar. Chem.* **1978**, *6*, 77−85.
(23) DeGrandpre, M. D.; Hammar, T. R.; Smith, S. P.; Sayles, F. L. *Limnol. Oceanogr.* **1995**, *40*, 969−975.
(24) Martz, T. R.; Carr, J. J.; French, C. R.; DeGrandpre, M. D. *Anal. Chem.* **2003**, *75*, 1844−1850.
(25) Dickson, A. G. *Deep Sea Res.* **1981**, *28A*, 609−623.

A_T is total alkalinity of the sample. The right-hand side of eq 1 represents the difference in proton donors (HA) and acceptors (B) in a titration mixture containing n donors and m acceptors. The indicator is also an acid−base species and must therefore enter into the proton balance. Based on Dickson's definition, we added the term $[I^{2-}]$ to the summation of proton acceptors in eq 1.

In the analysis, sample in a stirred flow cell is gradually displaced by titrant. The mixture of titrant and sample occupying the flow cell at any given time has a constant internal mass (given that the ionic backgrounds match), M_T,

$$M_T = M_{a/i} + M_s \tag{2}$$

Substitution of M_T into the left side of eq 1 gives

$$\frac{C_{a/i}M_{a/i} - A_T M_s}{M_T} = C_{a/i}\frac{M_{a/i}}{M_T} - A_T\frac{M_s}{M_T} \tag{3}$$

The mass ratios in eq 3 are the dilution factors of the titrant ($f_{a/i}$) and sample (f_s)

$$f_{a/i} = M_{a/i}/MT \quad \text{and} \quad f_s = M_s/M_T \tag{4}$$

The dilution factor $f_{a/i}$ is calculated from the ratio of total indicator concentration in the flow cell, $[I]_T$, to the total indicator concentration in the titrant, $[I]_{a/i}$, which is equal to the ratio of moles of H^+ added, $[H^+]_{added}$, to initial titrant concentration, $C_{a/i}$

$$f_{a/i} = \frac{M_{a/i}}{M_T} = \frac{[I]_T}{[I]_{a/i}} = \frac{[H^+]_{added}}{C_{a/i}} \tag{5}$$

The relationship described by eq 5 is the primary innovation of TMT: the indicator determines the amount of titrant added ($[H^+]_{added}$) while simultaneously establishing the equilibrium position (pH) of the titration mixture. Utilizing the indicator as a tracer eliminates volumetric measurements, shifting the burden of analytical performance to the spectrophotometer.

Conventional seawater A_T measurements are not based on an end point but, rather, use a mass balance on the hydrogen ion in combination with titration data to determine the best-fit value of A_T to the data.[25] In this application, the alkalinity balance is modified to include the dilution factors and indicator equilibrium

$$A_T f_s + [H^+] + [HSO_4^-] + [HF] - [OH^-] - 2[CO_3^{2-}] - [HCO_3^-] - [I^{2-}] - C_{a/i}f_{a/i} = 0 \tag{6}$$

where I^{2-} is the deprotonated form of BCG and HSO_4^- and HF are other non-CO_2 acid−base species that contribute to the proton mass balance in seawater at low pH. Using each species' equilibrium expressions, mass balances, and the fact that $f_{a/i} + f_s = 1$, eq 6 rearranges, giving

$$A_T(1 - f_{a/i}) + [H^+] + \frac{S_T(1 - f_{a/i})}{1 + K_s/[H^+]} + \frac{F_T(1 - f_{a/i})}{1 + K_F/[H^+]} - \frac{K_w}{[H^+]} - \frac{2C_T(1 - f_{a/i})K_1K_2}{[H^+]^2 + K_1[H^+] + K_1K_2} - \frac{C_T(1 - f_{a/i})K_1[H^+]}{[H^+]^2 + K_1[H^+] + K_1K_2} - [I^{2-}] - C_{a/i}f_{a/i} = 0 \tag{7}$$

where $C_T = [CO_2(aq)] + [H_2CO_3] + [HCO_3^-] + [CO_3^{2-}]$, K_1 and K_2 are the first and second dissociation constants of carbonic acid, respectively, and K_s and K_f are the dissociation constants of HSO_4^- and HF, respectively. Temperature-dependent equilibrium constants for seawater (except for the indicator) were taken from DOE.[26] K_1 and K_2 in 0.7 mol kg·soln^{-1} NaCl were taken from Dyrssen and Hansson.[27] Total sulfate, S_T, and total fluoride, F_T, are calculated from their conservative relationship with salinity. For Na_2CO_3 and NaOH samples, $S_T = F_T = 0$. $[I]_T$, $[H^+]$, and $f_{a/i}$ are calculated from absorbance data, as described below, leaving A_T and C_T as the two unknowns in eq 7. A "residual" value is calculated for each titrant addition, using eq 7. A_T and C_T are then calculated from a set of absorbance and temperature data using a nonlinear least-squares calculation (NLLS), which minimizes the sum of the squares of the residuals, $\sum$residual^2, by iteratively optimizing A_T and C_T.[25] The Excel spreadsheet used to calculate A_T contains a combination of cell formulas and Visual Basic routines that perform the NLLS calculation for each set of titration points. The key in using the NLLS approach is to collect a sufficient number of measurements in the most trusted range of the instrument and chemical model, giving an overdetermined problem. Good initial guesses of the unknown parameters then ensures convergence on their actual values. The total alkalinity TMT in this paper uses ~25−30 different equations (one for each titration point) to solve for the two unknowns (A_T and C_T).

C_T is necessary in the NLLS calculation, but it needs to be constrained only to a reasonable range for the NLLS to determine A_T. The insensitivity to C_T is due primarily to the pH range used where nearly all of the carbonate species are in the form H_2CO_3 or CO_2(aq) and therefore do not enter into eq 6. In practice, C_T is known in almost all oceanographic locations to well within 10% which is adequate for the NLLS model.

Calculation of $[I]_T$ and $[H^+]$ for a Titration Point. The calculations described above require individual concentrations of each form of the indicator for each titration point in order to calculate the total indicator concentration ($[I]_T$), dilution factors and pH of the solution. BCG is a diprotic molecule with p$K_{a1} \ll 0.0$ [28] and p$K_{a2} \sim 4.5$, where K_{a1} and K_{a2} are the first and second dissociation constants, respectively. Above a pH of ~0, only the second dissociation is important

$$HI^- \underset{K_a}{\rightleftharpoons} H^+ + I^{2-} \tag{8}$$

The equilibrium and mass balance equations are

$$K_a = [H^+][I^{2-}]/[HI^-] \tag{9}$$

$$[I]_T = [HI^-] + [I^{2-}] \tag{10}$$

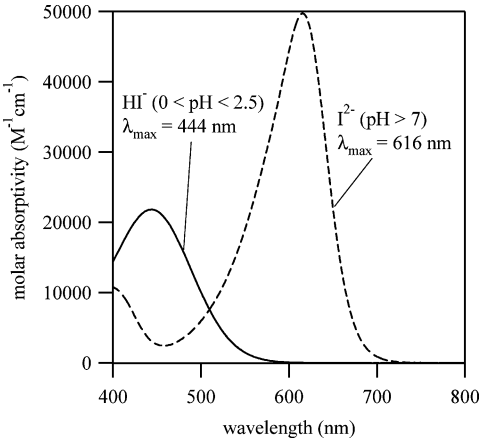

Figure 1. Absorbance spectra of singly protonated (HI^-) and fully deprotonated (I^{2-}) BCG. Absorbance maximums are at 444 and 616 nm for HI^- and I^{2-}, respectively. These scans were obtained on a Cary 300 with a spectral band-pass of 1 nm and optical path length of 1 cm. As described in ref 33, BCG molar absorptivities may vary slightly between dye lots.

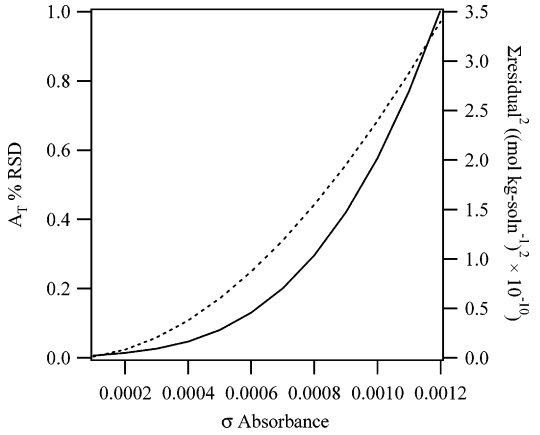

Figure 2. Theoretical precision plots of A_T % RSD (solid line) and Σresidual^2 (dotted line), showing the instrumental performance in relation to absorbance precision. Using this plot and the desired A_T precision of 2 μmol kg·soln^{-1} (0.1% RSD), the benchmark for absorbance precision was set at $\leq \pm 0.0005$. Based partly on this plot and partly on experimental data (see text), the maximum acceptable Σresidual^2 was set to $\leq 7 \times 10^{-10}$.

where K_a is the second ionic strength-dependent dissociation constant (i.e., concentration constant) (K_{a2}).

As shown in Figure 1, the HI^- $\lambda_{max} = 444$ nm and the I^{2-} $\lambda_{max} = 616$ nm. Absorbance (A) at a particular wavelength (λ) is given by

$$_{\lambda}A = {}_{\lambda}\epsilon_{HI} b[HI^-] + {}_{\lambda}\epsilon_{I} b[I^{2-}] \tag{11}$$

where ϵ is the molar absorptivity of each species at wavelength λ and b is the path length. In general, the indicator spectra overlap, and therefore, $_{\lambda}A$ has contributions from both forms at each analytical wavelength. The actual analytical wavelengths used in the TMT were 440 and 620 nm (see Experimental Section, under heading Titration Apparatus). The indicator species are calculated using

$$[HI^-] = \frac{{}_{440}A_{620}\epsilon_I b - {}_{620}A_{440}\epsilon_I b}{{}_{440}\epsilon_{HI} b_{620}\epsilon_I b - {}_{440}\epsilon_I b_{620}\epsilon_{HI} b} \tag{12a}$$

$$[I^{2-}] = \frac{{}_{620}A_{440}\epsilon_{HI} b - {}_{440}A_{620}\epsilon_{HI} b}{{}_{620}\epsilon_I b_{440}\epsilon_{HI} b - {}_{440}\epsilon_I b_{620}\epsilon_{HI} b} \tag{12b}$$

For a mixture of two molecules with overlapping absorbance spectra at two analytical wavelengths, the numerical solution of the speciation requires four molar absorptivity values, one at each wavelength for each species. Equations 12a and 12b are used with eq 9 to calculate $[H^+]$ and with eq 10 to calculate $[I]_T$. $[I]_T$ and $[I]_{a/i}$ are then used with eq 5 to obtain the dilution factors, $f_{a/i}$, and f_s. These calculations require accurate pK_a, ϵ, and path length. It is convenient to combine ϵb into a single parameter, as described in the Experimental Section below.

TMT Simulation Model. A mixing model was combined with an equilibrium model based on the A_T balance (eq 6) to examine the sensitivity of TMT precision and accuracy to different parameters. A simple one-tank dilution model agreed well with observed dilution data. Systematic and random errors were applied to absorbances and other parameters generated in the mixing model, and then A_T was calculated from the least-squares solution to a set of equations based on eq 7. The model was used to evaluate the importance of different titration parameters such as dilution factor (i.e., a/i ratio in titrant), path length, absorbance limits, absorbance noise, and nominal pump volume.

Titration precision was investigated as a function of the absorbance and temperature precision. As seen in Figure 2, as absorbance precision deteriorates A_T precision quickly degrades. Absorbance precision must be less than ± 0.0005 AU to achieve our goal of 0.1% A_T precision. Thermostating fluctuations also affect precision because the temperature dependence of each constant (especially indicator pK_a) is not perfectly known (see Experimental Section). Because an error in pK_a of 0.01 leads to an A_T error of $\sim$15 μmol kg·soln^{-1} (see accuracy discussion below) it may be necessary to determine a more accurate, temperature-dependent pK_a for the second dissociation of BCG or thermostat to better than ± 0.05 °C in order to optimize the precision. ϵ, in contrast, is relatively insensitive to temperature instability. Even a 20% error in the temperature dependence of ϵ (slope of ϵ vs temperature) results in ≤ 0.1 μmol kg·soln^{-1} error in A_T over ± 0.15 °C, the estimated uncertainty of the temperature in the flow cell described below.

Sensitivity to systematic errors (accuracy) was examined both numerically and by propagation of error. A thorough discussion of the uncertainty is beyond the scope of this paper, but we discuss the most important results here. Indicator pK_a errors of +0.001 and +0.010 lead to A_T errors of +2 and +15 μmol kg·soln^{-1}, respectively. A_T errors due to errors in the titrant concentration ($C_{a/i}$) are dependent on the dilution factor (i.e., the a/i ratio) used in the TMT. With $f_{a/i} \sim 0.5$, a 10 μmol kg·soln^{-1} error in $C_{a/i}$ leads to a 11−14 μmol kg·soln^{-1} A_T error. Accuracy errors due to $C_{a/i}$ decrease with decreasing dilution factor, but limits in indicator solubility and optical path length restrict $[I]_T$ to a narrow range,

(26) Dickson, A. G., Goyet, C., Eds. *DOE Handbook of methods for the analysis of the various parameters of the carbon dioxide system in sea water*, Version 2; A. ORNL/CDIAC-74, 1994.
(27) Dyrssen, D.; Hansson, I. *Mar. Chem.* **1973**, *1*, 137−149.
(28) Aragoni, M. C.; Arca, M.; Crisponi, G.; Nurchi, V. M.; Silvagni, R. *Talanta* **1995**, *42*, 1157−1163.

and titrant pump volume constrains the number of titration points achievable at lower dilution factors. Temperature accuracy errors result in offsetting errors from pK_a and molar absorptivity. For example, a thermistor temperature error of +0.5 °C results in a A_T error of −1.6 μmol kg·soln^{-1} due to pK_a and +3.3 μmol kg·soln^{-1} due to ϵ for a combined error of +1.7 μmol kg·soln^{-1}. Systematic absorbance errors of ±0.001 or, conversely, molar absorptivity errors of 0.14% lead to A_T errors of ±5−6 μmol kg·soln^{-1}. Based on these sensitivity studies, it is clear that very high quality absorbance data, along with accurately known temperature dependence of pK_a are required to achieve the desired A_T precision and accuracy.

EXPERIMENTAL SECTION

Solution Preparation. All solutions were prepared gravimetrically, and weights were corrected for air buoyancy. Samples were immediately transferred from the preparation vessel to gas-impermeable bags to limit evaporation and gas exchange during sampling. All solutions containing indicator were carefully shielded from light. NaCl (biological grade certified, Fisher Lot 041477) was added to all solutions to set I = 0.700 mol kg·soln^{-1}.

Each alkalinity sample was prepared in a 7.5-L LDPE carboy, mixed for >1 h, and drained into a 10-L sterilized, inert, gas-impermeable bag (SCD, TC Tech). Sodium carbonate test samples were prepared using anhydrous Na_2CO_3 (Alfa Aesar Puratonic, 99.997% purity), dried at 280 °C for 3 h, and stored in a desiccator until use. Na_2CO_3 in NaCl was prepared to ∼0.0010−0.0013 mol kg·soln^{-1} by adding ∼0.77−0.93 g of Na_2CO_3, ∼7000 g of H_2O, and ∼297 g of NaCl. NaOH samples were prepared from Fisher standard NaOH (molarity, 0.10030 mol L^{-1}; ρ = 1.0027 g/mL). NaOH in NaCl was prepared to ∼0.00235 mol kg·soln^{-1} by adding ∼175 g of NaOH, 7000 g of H_2O, and ∼306 g of NaCl. The CRM is filtered and sterilized seawater prepared in Dickson's laboratory.[29]

A stock solution of BCG was prepared by dissolving ∼2 g of NaHBCG (dye content ∼90%, dye purity ∼95.4%, Sigma Aldrich dye lot 01920DI) in ∼2400 g of water to give $[I]_{stock}$ ∼1 × 10^{-3} mol kg·soln^{-1}. The stock was stored in an amber glass jug. All other indicator solutions were prepared from weighed amounts of this stock.

Titrant was prepared from standard HCl (Fisher Scientific, molarity, 0.099 80 mol L^{-1}; ρ = 0.9998 g/mL) and BCG stock by adding ∼450 g of stock, ∼150 g of HCl, ∼6000 g of H_2O, and ∼281 g of NaCl. Titrant was stored in a 10-L bag (SCD, TC Tech) and wrapped in black plastic to prevent light exposure.

Determination of ϵb. We determined the combined value, ϵb, by recording the absorbance of indicator solutions directly in the flow cell. In this way, ϵb accounts for the exact flow cell path length and band-pass of the detection system. ϵb values must be redetermined for each disassembly and reassembly of the flow cell because of slight changes in the positioning of the fiber optics. ϵb is quantified by measuring the absorbance of a solution in which the pH is set to maximize a single form of the indicator. For BCG, we first quantified the ϵb values for I^{2-} by measuring the absorbance of a basic solution (pH ∼10), where $[I^{2-}]$:$[HI^-]$ > 1 × 10^6. At low pH, it is impossible to isolate HI^- and absorbance measurements on acidified indicator (pH ∼2) must be corrected for the presence of I^{2-} using eqs 9 and 10 and the predetermined ϵb values of I^{2-}. The temperature dependence of ϵb is determined by recording absorbances at different temperatures. Because they are specific to our optical system, the ϵb results are not reported here.

Indicator pK_a. An accurate indicator pK_a is very important in the calculation of $[H^+]$ (eq 9) and, consequently, A_T. Despite equal ionic strengths, a Na_2CO_3 standard prepared in NaCl background requires a different pK_a value than a seawater CRM due to the formation of fewer ion pairs.[27] Because there is no reliable data reported for the pK_a of BCG in 0.7 mol kg·soln^{-1} NaCl, we relied on our own approximation for this value. We used data reported by others[30,31,32] to obtain a pK_a for the CRM titration.

The pK_a in NaCl background was determined by using the TMT system to titrate a Na_2CO_3 standard and iteratively refining A_T and pK_a to minimize the value $\sum$residual^2. We found pK_a(NaCl) = 4.475 with I = 0.700 mol kg·soln^{-1} at 22.00 °C. The pK_a at 25 °C on the free H^+ scale in molal units at salinity of 35‰ was reported by Byrne and co-workers in seawater (4.435)[30] and synthetic seawater (4.4166),[31] and by King and Kester in seawater (4.410).[32] We calculated A_T for the CRM using all three of these values, converted to the same concentration scale (mol kg·soln^{-1}), titration temperature, and corrected to the CRM salinity as described in ref 1.

The temperature dependence (i.e., the enthalpy of reaction, $\Delta H°$) for the pK_a of BCG has not been reported. The approximate $\Delta H°$ for BCG is found by observing changes in the absorbance ratio of a mixture of HI^- and I^{2-} as temperature is varied.[33] Because all work in this study was done over a relatively narrow temperature range, it is assumed that $\Delta H°$ is constant with temperature. We found that $\Delta H°$ = 3.0 kJ mol^{-1} for NaCl solutions and estimated $\Delta H°$ = 2.5 kJ mol^{-1} for the CRM, based on a combination of our data and that of Breland and Byrne.[31] From the Van't Hoff equation, the pK_a temperature dependence is −0.0018/°C in 0.7 mol kg·soln^{-1} NaCl and −0.0014/°C in seawater.

Titrant $C_{a/i}$. Accuracy ultimately depends on the titrant concentration, $C_{a/i}$. As pointed out earlier, $C_{a/i}$ is the *acidity* of the titrant due to both the HCl and the indicator in the mixture. We used a Na_2CO_3/NaCl solution as the primary standard for assigning $C_{a/i}$. The reliability of this procedure is thus only as accurate as the purity of the standard, the accuracy with which solutions are prepared, and the purity of salt added to the standard solution. As an independent verification with another primary standard, NaOH in NaCl (∼0.2 mol kg·soln^{-1}, I = 0.7 mol kg·soln^{-1}) was standardized against potassium hydrogen phthalate in NaCl (I = 0.7 mol kg·soln^{-1}) and used to titrate the a/i mixture with an electrode and accurate syringe pump (Kloehn Ltd.). The strong acid and weak acid equivalence points were located using Gran's method.[34] Values of $C_{a/i}$ obtained by Na_2CO_3 standardization and NaOH titration agreed within a few μmol kg·soln^{-1} when accounting for the NaCl impurity (see Results and Discussion).

Titration Apparatus. Solutions were titrated with the setup shown in Figure 3. Batch measurements are fully automated, requiring an operator only to reload samples. Sample and titrant

(29) Dickson, A. G.; Afghan, J. D.; Anderson, G. C. *Mar. Chem.* **2003**, *80*, 185−197.
(30) Byrne, R. H.; Robert-Baldo, G.; Thompson, S. W.; Chen, C. T. A. *Deep Sea Res.* **1988**, *35*, 1405−1410.
(31) Breland, J. A.; Byrne, R. H. *Deep-Sea Res. I* **1993**, *40*, 629−641.
(32) King, D. W.; Kester, D. R. *Mar. Chem.* **1989**, *26*, 5−20.
(33) Martz, T. R. Ph.D. Thesis, University of Montana, 2005.
(34) Pankow, J. F. *Aquatic Chemistry Concepts*; Lewis: Chelsea, MI, 1991; Chapter 10.

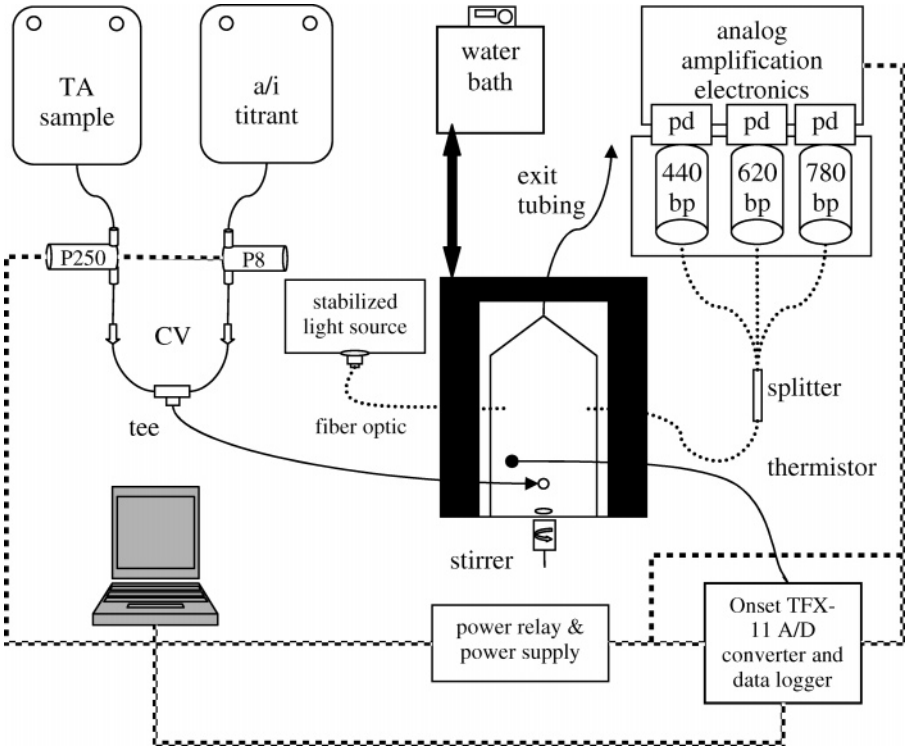

Figure 3. Schematic of the TMT titration apparatus. Sample and titrant are pumped by 250 (P250) and 8 μL (P8) solenoid pumps. Check valves (CV) prevent reverse breakdown of pump seals. Each pump output is coupled to a low dead volume tee, which connects to the flow cell below the light path. Light is collected at the return fiber and split to three dual band-pass filters (bp). The photocurrent from each photodiode (pd) is amplified using a simple two-stage inverting op-amp design. The resulting voltage is then digitized and logged by the TFX-11. Water bath temperature is set at 22.0 °C and connected to a built-in manifold in the flow cell. The temperature of the titration mixture is also directly monitored by a thermistor. A magnetic stir bar is sealed into the flow cell by an acrylic base plate, with a stirring motor mounted directly below.

bags are connected to 250 and 8 μL per pulse solenoid pumps (Bio-Chem Inc.), respectively. Pumps are pulsed on 0.5- (pretitration) or 1-s (titration) intervals for titrant and 2-s intervals for sample. The pump outlets merge at a low dead volume tee, which connects to the inlet of an insulated stirred optical flow cell with ~5-mL internal volume. All tubing leading up to the flow cell is 1.00-mm-i.d. PEEK.

The flow cell (Figure 3) has an integrated water manifold connected to a water bath (Thermo Neslab; ±0.01 °C) for temperature regulation. A thermistor, installed in the flow cell inner chamber, directly monitors temperature of the titration solution with 0.01 °C resolution. The internal temperature was stable to ~0.10−0.15 °C. As discussed above, this level of temperature stability affects precision, but using temperature-dependent equations for ϵb and equilibrium constants adequately reduced the temperature sensitivity.

The instrument design described here uses active mixing rather than static mixing such as a mixing coil or commercially available in-line mixer used in FIA and HPLC. Earlier studies with static mixing found that concentration and pH gradients between the source fiber and the return fiber optic led to deviations from Beer's law and large errors in A_T. Active mixing has distinct advantages over a static mixer for the initial laboratory proof-of-concept stage of TMT. Active mixing eliminates gradients within the optical path, resulting in dramatically improved performance. Also, the mixing model for a stirred cell is simple and agrees with observed data. Finally, active mixing helps reduce any dead volume within the reaction chamber, guaranteeing a complete flush of each new sample.

The optical system and analog electronics used in this study are similar to those described by DeGrandpre et al.[23] The optical system consists of a tungsten−halogen source with optical feedback (Custom Sensors, 55T), 1000-μm core fused-silica fiber optics (Edmond Scientific), a three-way fiber-optic bundle splitter (FiberTech Optica), and a three-channel spectrophotometer built from dual band-pass filters (Intor) and Si photodiodes (S2386-45K, Hamamatsu) interfaced to a custom-built amplifier board (Sunburst Sensors LLC). The center wavelength (CWL) of the band-pass filters was only available on 5-nm intervals, so the filters were selected to match peak absorbance wavelengths of BCG as closely as possible (440- and 620-nm CWL filters for λ_{max} at 444 and 616 nm, respectively; Figure 1). The full width at half-maximum of the band-pass filters is 10 nm. Absorbances measured at a reference channel (780 nm) are subtracted from the analytical absorbances to account for baseline offsets (e.g., due to air bubbles). Adding a second identical filter to each channel reduced off-band radiation (i.e., stray light) to negligible levels. At each channel, a photodiode is mounted on the other side of the two filters and directly connected to the analog board. Improvements in the optical design and additional signal averaging increased the S/N from ~3000 to ~5000 (~0.0001 AU), where it is limited primarily by the resolution of the 12-bit A/D converter. A TFX-11 microcomputer (Onset Corp.) controls pumps, analog to digital conversion, and data acquisition.

As discussed above (see Figure 2), very stable and precise absorbances (<0.0005 AU) are required for this application. Absorbance reproducibility better than ±0.001 AU is very difficult to achieve on a single-beam instrument. To obtain the highest

quality data requires a very short time between blank and sample measurements, but our system records absorbance several minutes after the blank due to the time required to flush the cell. The nonabsorbing reference wavelength (i.e., 780 nm, Figure 1) provides short-term corrections for source noise and air bubbles but cannot account for the wavelength-dependent drift exhibited by a tungsten light source over minute-long periods. The light source we selected is stabilized by optical feedback and exhibited very little drift over the time intervals between blank and sample (drift ~0.0001 AU h^{-1}).

Titrations. All titrations were carried out with the water bath set to 22.0 °C. A titration begins with a ~110-mL flush of the alkaline sample. After a blank (100% T) reading is obtained from this solution, the 8-μL titrant pump delivers a pretitration volume (~1.5 mL in 90 s with 0.5-s pulses) to move the titration closer to the equivalence point. The microcomputer constantly monitors absorbance and spectrophotometric pH, comparing real-time values with preset limits for the remainder of the titration. Next, titrant is added in medium increments (~150 μL in 10 s with 0.5-s pulses) to save time while reducing the pH to ~6. Titrant is then added in single 8-μL increments with a 0.5-s pause for stirring, and a data point is recorded for each addition. The titrations are not dependent on the exact volume delivered, but small-volume increments are required to obtain enough titration points for the NLLS calculation. When the solution in the mixing chamber reaches pH 3.5, data acquisition stops and the 250-μL sample pump begins the next flush. The sample flush and titration require 14 and 2.5 min, respectively.

We evaluated accuracy and precision with the high-salinity alkaline standards described above. The titration data are imported into Excel for filtering and calculation of A_T. The absorbance data are filtered according to preset limits on reference absorbance (i.e., optical blank), analytical absorbance range, pH range, and magnitude of the residual value. The first data filter removes any point where ${}_{780}A > 0.0015$. Then all data are removed that fall outside of the range $3.5 < \text{pH} < 3.8$ and $0.1 < A < 1.0$. A_T is calculated from the resulting set of residuals. If any point's squared residual value exceeds 2.5×10^{-11} (corresponding to a residual error of 5 μmol kg·$soln^{-1}$), the point is ignored. This threshold is based on the TMT model, which predicts that ± 5 μmol kg·$soln^{-1}$ is outside the 3σ (99.7%) probability for a system with absorbance noise of $<\pm 0.0005$. Absorbance noise larger than 0.0005 is typically caused by bubbles in the optical path. With these points removed, A_T is recalculated. If, after the recalculation, $\sum\text{residual}^2 > 7 \times 10^{-10}$, then the entire titration is rejected. The $\sum\text{residual}^2$ limit is obtained using the theoretical model and a Monte Carlo approach (Figure 2) in combination with experimental observation. The number 7×10^{-10} was selected as an acceptable upper limit for the sum of squared residuals from 25 to 30 titration points. Manual rejection of titration data was always avoided to retain the automated nature of the system.

RESULTS AND DISCUSSION

Absorbance Precision and Stability. Before titrating samples, the optical system's absorbance reproducibility was evaluated by recording replicate absorbance measurements on an indicator solution. This step served to verify that precise values of ϵb and absorbance could be obtained and that path length did not change with time. Figure 4 shows that the stability of replicate absorbance measurements is around ±0.0003 AU at 0.7 AU (RSD = 0.04%; $n = 34$). Based on our model predictions (Figure 2), 0.04% AU precision leads to 0.024% (0.6 μmol kg·$soln^{-1}$) A_T precision, which is adequate for seawater A_T analysis. The full range of absorbance scatter in Figure 4 (~0.001 or ~3σ) corresponds to ~10 μmol kg·$soln^{-1}$ in A_T.

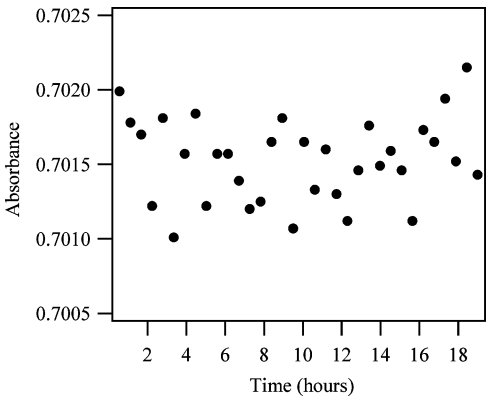

Figure 4. Absorbance precision and stability of the optical detection system shown in Figure 3. Absorbance reproducibility was tested by running full system flushes of a blank (0.7 mol kg·$soln^{-1}$ NaCl) and an I^{2-} solution (19 μmol kg·$soln^{-1}$ I^{2-}, pH 10.6, 0.7 mol kg·$soln^{-1}$ NaCl) repeatedly back-to-back for ~19 h. A complete flush of the flow cell takes ~14 min; leading to 28 min per absorbance measurement. The 1σ measurement precision of the instrument is ±0.0003 ($n = 34$) at 620 nm when $A = 0.7015$ (RSD = 0.04%).

Titration Data. Figure 5A shows the absorbance data collected during a single titration. The first five points are blank values. Blank data are not shown because the noise (±0.0001) is not readable on the scale shown in Figure 5A. Indicator species (Figure 5B, right axis) are calculated using eq 12. $[H^+]$ (Figure 5B, left axis) is calculated from eq 9. Carbonate species (Figure 5B, left axis) are calculated from the CO_2 equilibrium equations, $[H^+]$, and C_T. pH is also shown (Figure 5C) to illustrate the dynamic range of BCG. Following Figure 5C, the first large pretitration pulse brings the titration solution to a pH of 6.0−6.5. Since this is ~2 units higher than the pK_a of BCG, the absorbance is high at 620 nm and low at 440 nm (Figure 1, Figure 5A). Almost all of the 440-nm absorbance just after the blank (data acquisition number <20) is due to the I^{2-} form of BCG, which weakly absorbs at this wavelength. As titrant is added, the decreasing pH reflects the increasing acidity of the mixture inside the flow cell. In Figures 5A and 5C, the overlapping absorbance and pH range used to calculate A_T is outlined in boxes. As described below, set pH limits determined the range of data used for residual calculations. After filtering, absorbance and dilution factor ($f_{a/i}$) ranged from 0.12 to 0.58 AU and 0.40−0.60, respectively, depending on the sample A_T. For example, when A_T ~2000 μmol kg·$soln^{-1}$, ${}_{440}A = 0.46-0.54$, ${}_{620}A = 0.12-0.21$, and $f_{a/i} = 0.40-0.55$; and when A_T ~2500 μmol kg·$soln^{-1}$, ${}_{440}A = 0.50-0.58$, ${}_{620}A = 0.13-0.23$, and $f_{a/i} = 0.46-0.60$.

Figure 6 shows the residuals calculated using eq 7 for a single titration (Figure 5). The pH was restricted to a narrow range because the residual set was not flat over the selected absorbances. The cause of the residual trends at high and low pH is unclear. Negative residuals at pH >4.0 may be due to slow H_2CO_3 dehydration (which affects eq 7 by changing $[H^+]$ and C_T), while at pH <3.5 they may be due to spectrophotometer absorbance accuracy limits. The section of residuals with least slope

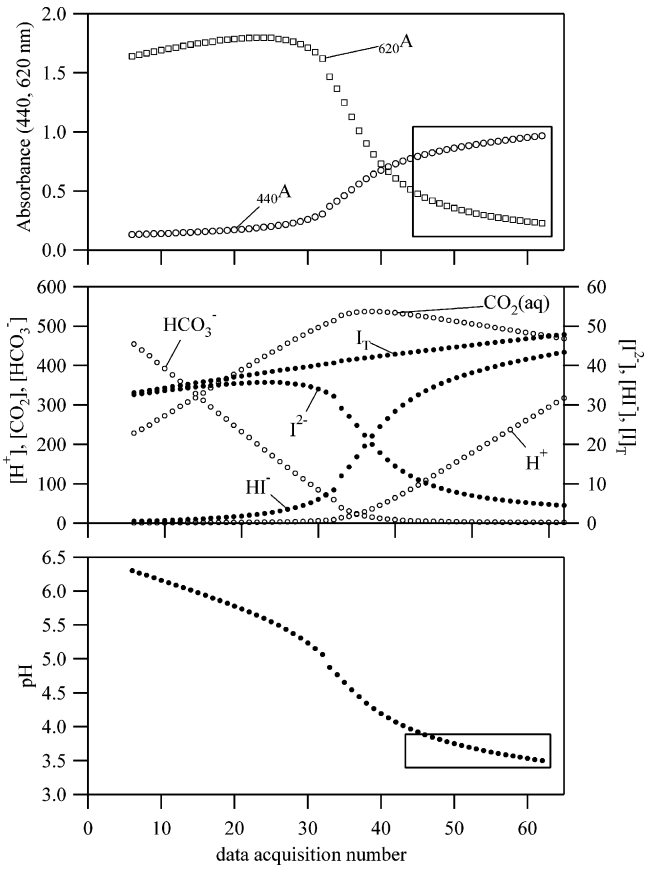

Figure 5. Measurement profiles for a single tracer monitored titration. (A) absorbance data are collected at analytical wavelengths of 440 and 620 nm, near the absorbance peaks of BCG. (B) Speciation of the titration is shown for all molecules or ions present in significant amounts. Concentrations are in μmol kg·soln^{-1}. (C) pH calculated from the absorbance data in (A). Rectangles are drawn around the absorbance and pH ranges used to calculate A_T.

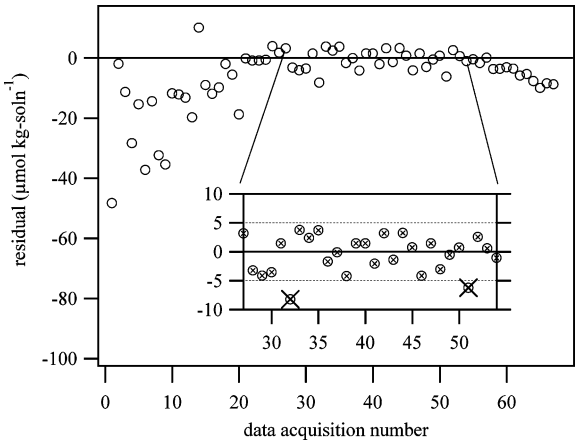

Figure 6. Residuals for a single titration calculated using eq 7, as described in the Theory section. The entire data set (circles) was filtered to the overlapping range 3.5 < pH < 3.8 and 0.1 < A < 1.0 (circles with small ×, inset). Secondary filters reject points where $_{780}A$ > 0.005 or $\sum$residual^2 > 2.5 × 10^{-11} (circles with large ×, inset). A typical set of data is narrowed down from the initial 60−70 points to ∼20 points. As sample A_T increases, the absorbance range and pH range remain the same, but the dilution factor and hence total indicator concentration operate over different ranges (see text).

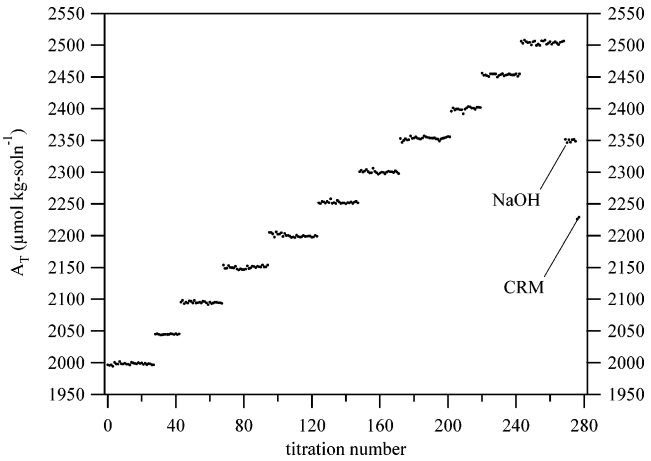

Figure 7. Results from 279 titrations spanning the oceanic range of total alkalinity. The primary standard Na_2CO_3 in 0.7 mol kg·soln^{-1} NaCl was used as the principal analyte in this study. A NaOH secondary standard was run to verify the accuracy. The method was also checked against a seawater CRM. Note that Na_2CO_3 samples are plotted in order of increasing A_T but were not analyzed in this order (see Figure 9).

and values near zero corresponds to the optimal range in absorbance and pH (Figure 6, inset; Figure 5, boxes).

As stated earlier, residual outliers within the optimal pH and absorbance range are most likely due to air bubbles. Air bubbles in the flow cell are not identifiable directly from the analytical absorbance data, but manifest through increased noise at the reference channel at 780 nm and individual residual values outside the range ±5 μmol kg·soln^{-1}. The filtering described above typically resulted in less than five rejected measurement points for accepted titrations. Greater than five outliers (increased air bubbles) usually resulted in rejection of the analysis due to exceeding the $\sum$residual^2 limit. We found that adding back pressure at the cell outlet to eliminate air bubbles helped reduce outliers but resulted in impractical flush times.

Total Alkalinity Replicates: Accuracy and Precision. From the original set of 316 titrations, 37 were rejected because their $\sum$residual^2 value exceeded 7 × 10^{-10} (loss rate of ∼10%). Relaxing the filter criteria to $\sum$residual^2 > 7 × 10^{-10} to accept more residual outliers reduced the number of rejected titrations but significantly affected the titration precision. Figure 7 shows the results of the remaining 279 titrations performed on 13 different samples. Eleven Na_2CO_3 standards (I = 0.7 mol kg·soln^{-1}, NaCl) with ∼50 μmol kg·soln^{-1} increments over the range 2000−2500 μmol kg·soln^{-1} were analyzed, encompassing the entire oceanic range of A_T.[35] The uncertainty in the preparation of these solutions is 1−2 μmol kg·soln^{-1}. We also titrated a seawater CRM, a standard widely used to verify the performance of seawater alkalinity systems.[36] Figure 8 shows the linearity of the instrumental response, along with 1σ error bars. Standard deviations for each sample ranged from ±0.6 to ±2.7 μmol kg·soln^{-1} (Table 1). The TMT response is linear (R^2 = 0.9999) over the oceanic range of A_T and thus requires no calibration of the response beyond assigning pK_a, $C_{a/i}$, and ϵb.

Table 1 gives the measured and standard A_T values for each solution. Based on the pooled standard deviation of 279 titrations, the 1σ precision is ±2.1 μmol kg·soln^{-1} (0.1%) and accuracy is ∼±4.0 μmol kg·soln^{-1} (∼0.2%). The sensitivity of the CRM

(35) Millero, F. J.; Lee, K.; Roche, M. *Mar. Chem.* **1998**, *60*, 111−130.
(36) Dickson, A. G. *Oceanography* **2001**, *14* (4), 21−22.

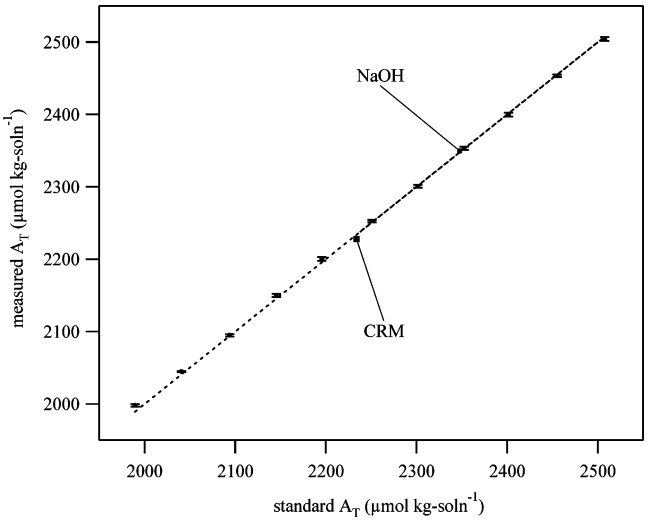

Figure 8. Averaged results from Figure 7 with errors (1σ) show the linear response ($R^2 = 0.9999$) of the TMT method. The dashed line is a 1:1 line. Standard A_T is calculated from the solution preparation, as described in the Experimental Section. Over the range 2100−2500, the TMT was accurate to ~4 ± 2 μmol kg·soln^{-1}.

Table 1. Results of 279 Titrations on Total Alkalinity (units in μmol kg·soln^{-1})[a]

batch	N	measured average	sd	prep A_T	error
Na_2CO_3(1)	28	1998.1	1.6	1989.3	8.8
Na_2CO_3(2)	15	2044.8	0.6	2040.7	4.1
Na_2CO_3(3)	25	2095.0	1.6	2093.7	1.3
Na_2CO_3(4)	27	2150.1	2.3	2145.2	4.9
Na_2CO_3(5)	29	2200.3	2.7	2195.5	4.8
Na_2CO_3(6)	24	2252.4	1.8	2250.9	1.5
Na_2CO_3(7)	24	2300.4	2.1	2301.4	−1.0
Na_2CO_3(8)	30	2353.3	2.3	2352.3	1.0
Na_2CO_3(9)	19	2399.8	2.7	2401.4	−1.6
Na_2CO_3(10)	23	2453.4	1.6	2454.9	−1.5
Na_2CO_3(11)	26	2504.1	2.5	2507.3	−3.2
NaOH	7	2349.8	2.2	2347.4	2.4
CRM 68 [30]	2	2217.5	1.6	2233.7	−16.2
CRM 68 [31]	2	2227.8	1.8	2233.7	−5.9
CRM 68 [32]	2	2256.4	2.3	2233.7	22.7

[a] The pooled standard deviation for the entire set is 2.1 μmol kg·soln^{-1}. CRM superscripts refer to the literature reference from which BCG pK_a was taken.

analysis to indicator pK_a is demonstrated by using three different literature values for the pK_a. The values calculated for the CRM span a A_T range of ~40 μmol kg·soln^{-1}. As explained in the theoretical model section above, the extreme sensitivity to indicator pK_a is a result of its importance in the residual (eq 7), where [H$^+$] is calculated using eq 9. The best agreement between the known CRM A_T and our measurement is from the pK_a reported by Breland and Byrne.[31] To achieve the desired accuracy, TMT requires a pK_a accurate to ~0.001 (see TMT Simulation Model in Theory section), but indicator pK_a determinations are typically accurate to ~0.01. Consequently, we expect that high accuracy (~2 μmol kg·soln^{-1}) seawater A_T measurement by TMT will require a slight adjustment to the indicator pK_a, based on preliminary CRM titrations.

Figure 9 shows the errors between measured and standard A_T values as a function of A_T (A) and time (B) for the set of averaged titrations (Figure 8) plus an additional average of seven

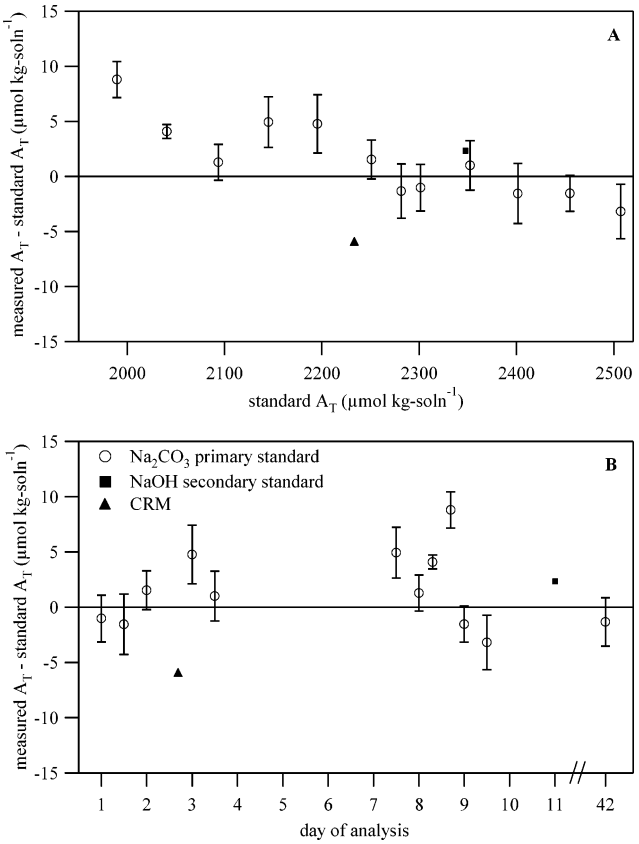

Figure 9. A_T errors from data in Figure 8 relative to (A) standard A_T and (B) time of analysis. Error bars (1σ) are shown for the carbonate standards. A Na_2CO_3 standard, freshly prepared and measured 42 days after the sampling began, shows that the system is extremely stable over long time periods without calibration. The trend in (A) is due to NaCl impurity in the titrant.

titrations on day 42 (A_T = 2283 μmol kg·soln^{-1}). Errors in measured A_T decrease from positive to negative as A_T increases (Figure 9A). The samples were not run in sequence of increasing or decreasing A_T, and Figure 9B shows that the trend in Figure 9A is not due to a time-dependent drift. This negative trend is most likely caused by a protic impurity in the titrant because this effect should vary with A_T. Titrations have increasing dilution factors with increasing A_T and a protic impurity will have a different effect at a different dilution factor, similar to a conventional titration with an impurity in the titrant. The TMT model predicts that acidic impurities in the titrant on the order of 20 μmol kg·soln^{-1} would result in the trend shown in Figure 9A. The observed errors in Figure 9 are actually less than 20 μmol kg·soln^{-1} because the impurity was also present in the standards used to assign $C_{a/i}$ (see Experimental Section). As expected, the zero crossing shown in Figure 9A (~2250−2350 μmol kg·soln^{-1}) corresponds closely with the solution used to assign $C_{a/i}$ (Na_2CO_3 No. 7, 2301.4 μmol kg·soln^{-1}). As mentioned in the Experimental Section, independent measurement of $C_{a/i}$ revealed an acidic impurity in the NaCl of ~20 μmol kg·soln^{-1}. This level of contamination also closely corresponds with the value reported on the Fisher Scientific Certificate of Analysis for the NaCl lot used. This error can be avoided by using purified NaCl[29] and further developing the rigorous, independent determination of $C_{a/i}$ described above (see section Titrant $C_{a/i}$). For an estimate of TMT performance in the absence of the titrant impurity, we applied a

correction of −1.9 μmol kg·soln^{-1} per 100 μmol kg·soln^{-1} of A_T to the data shown in Figure 9A. The Figure 9A corrected data are randomly distributed about the zero line over the range +2.5 to −3.3 with a standard deviation of 1.7 μmol kg·soln^{-1}.

The system sustained excellent accuracy and precision over the 11 days that the initial samples were analyzed and exhibited no detectable drift after more than a month. As shown in Figure 9B, 42 days after the first sample analysis, a new Na_2CO_3 standard was measured with accuracy and precision of 0.06 and 0.10%, respectively. All results were obtained with the same batch of titrant, without redetermination of ϵb or $C_{a/i}$, implying that the optical band-pass and path length are very stable. The absence of a time-dependent drift also demonstrates that the acid/indicator solution is chemically stable. Since the system is capable of fully automated drift-free operation (limited only by titrant consumption), the 10-L titrant bag used in this study could potentially titrate continuously for about five weeks, calibration-free, supplying over 3000 titrations on 16.5-min intervals.

CONCLUSION

Using TMT, we obtained highly precise and accurate, drift-free measurements with an automated titration system using low-precision pumps. Rather than volume, mass, or flow reproducibility, the titration performance depends instead upon spectrophotometric precision and stability. These results are exciting because the methodology offers a simplified approach to automated titrations. The accuracy and precision of the technique are ~0.2 and 0.1%, respectively, for carbonate standards in the range 2100−2500 μmol kg·soln^{-1}, corresponding to the observed oceanic range of A_T. The apparatus is fully automated, with sample throughput of ~90 day^{-1}. TMT performance currently approaches the performance of existing techniques for seawater A_T titration but with a greatly simplified apparatus. Precision of better than ±1 μmol kg·soln^{-1} has been achieved in shore-based laboratories by both spectrophotometric[1] and potentiometric[29] procedures, but both require meticulous quantification of either volume or mass. At-sea precision of <±2 μmol kg·soln^{-1} is unusual.

Although ±2 μmol kg·soln^{-1} in ~2300 μmol kg·soln^{-1} (0.1%) can be considered excellent precision for any titration, there remains some room for improvement. Because flush time dictates the time between analyses, a more efficient flow design could easily triple the sample throughput. The flow design must also be optimized to avoid generation of bubbles to reduce the number of discarded analyses. A static mixing design may be better suited for unattended operation. Unfortunately, incorporating a static mixer into TMT is difficult because the method is highly dependent on Beer's law calculations, which are not valid across concentration gradients. A diode array spectrophotometer offers an alternative method of $[I]_T$ calculation, via the isosbestic wavelength. The analytical wavelengths would also correspond closely with the peak absorbance wavelengths (~1 nm), which would allow intercomparison between different instruments using the same type of diode array and path length and also allow direct instrumental verifications such as wavelength and photometric accuracy.

As stated in the abstract, TMT is not limited to acid−base systems and can be generalized for use in other types of titrations. The tracer can be either an inert chromophore or an indicator that also serves as the sensing mechanism for the titration. In the latter, the primary requirement is that all forms of the indicator absorb light so total indicator concentration may be observed at any point in the titration from the sum of the different species (e.g., protonated + unprotonated; complexed + uncomplexed; reduced + oxidized). Several redox indicators exhibit a color change from blue to red when reduced. Many metal ion indicators have an absorbance spectrum in the visible region for both the free indicator and the indicator−metal ion complex. For example, a titration analogous to the one presented here could be accomplished by adding a quantitative amount of calmagite (a metal ion indicator with colored complexed and uncomplexed forms) to standardized EDTA and titrating Ca^{2+}. TMT also extends beyond absorbance spectrophotometry to fluorescence (provided that the excitation source remains constant and low concentrations are used where concentrations are calculated directly from fluorescence emission power[37]) since indicators with two fluorescing forms are commonly used in acid−base, redox, and metal ion titrations. If using an inert tracer, an alternative method (e.g., electrode) for observations on the equilibrium position of the titration would be required. We plan to test TMT in redox or complexometric titrations in the future to verify the general applicability of the method. In the near term, we plan to field test the TMT system, measuring A_T from shipboard underway seawater and continue working toward a fully autonomous TMT sensor for seawater A_T.

(37) Skoog, D. A.; Holler, F. J.; Nieman, T. A. *Principles of Instrumental Analysis*., 5th ed.; Harcourt & Brace: Chicago, 1998.

ACKNOWLEDGMENT

We thank Cory Beatty for technical assistance and Big Sky Machining for building the flow cell. This work was supported by National Science Foundation grant OCE-0327763 and Office of Naval Research grant N00014-00-1-0573.

Received for review September 8, 2005. Accepted December 23, 2005.

AC0516133